

Interplay between spin-orbit coupling and van Hove singularity in the Hund's metallicity of Sr_2RuO_4

Hyeong Jun Lee,^{1,2,3} Choong H. Kim,^{2,3,*} and Ara Go^{1,4,†}

¹Center for Theoretical Physics of Complex Systems, Institute for Basic Science (IBS), Daejeon 34126, Republic of Korea

²Center for Correlated Electron Systems, Institute for Basic Science (IBS), Seoul 08826, Republic of Korea

³Department of Physics and Astronomy, Seoul National University, Seoul 08826, Republic of Korea

⁴Department of Physics, Chonnam National University, Gwangju 61186, Republic of Korea

(Dated: November 12, 2020)

We investigate the roles of spin-orbit coupling and the van Hove singularity in the dynamical properties of Sr_2RuO_4 , which become prominent at zero and very low temperature, by means of density functional theory plus dynamical mean-field theory with an exact diagonalization solver. We examine the crossover between a Fermi liquid and a Hund's metal for a wide range of temperatures and Hund's coupling. In the absence of doping, we confirm that the Fermi liquid persists at zero temperature even with nonzero Hund's coupling. The freezing-moment mechanism suggests that thermal fluctuations lead to a suppression of the Fermi liquid phase and promote Hund's metallicity with incoherence. We show that the van Hove singularity is an additional key ingredient to drive the suppression at very low temperature by observing a doping dependence of the freezing or long-lived paramagnetic moments. The role of spin-orbit coupling is marked by an amplified Van Vleck contribution of spin susceptibility, significantly promoting Hund's metallicity. Together with the known doping dependence of Hund's metallicity, the additional VHS doping dependence found here may allow for the control of the Hund's metallicity of Sr_2RuO_4 (t_{2g}^4) by a fine tuning of the doping or possibly even strain.

I. INTRODUCTION

The recent discovery of Hund's metals promotes the importance of Hund's coupling in correlated multi-orbital systems.¹⁻³ While Hund's coupling can appear to reduce correlations by suppressing the Mott phase, it also enhances another type of correlation that exhibits various characteristic behaviors—for example, large renormalization masses depending on filling,^{4,5} spin (or J) freezing,^{6,7} and non-Fermi liquid.⁶ Furthermore, a strong Hund's coupling in multi-orbital systems induces significant orbital-selective behaviors.⁸⁻¹² As the name implies, the aforementioned characteristics of Hund's metals originate from local correlation effects.

Strontium ruthenate, Sr_2RuO_4 , is a well-known correlated metal¹³⁻²⁵ that undergoes a crossover from Hund's metal to Fermi liquid as the temperature drops.²⁶⁻²⁸ It exhibits unconventional superconductivity below 1.5 K,²⁹⁻³³ the precise mechanism of which is still under debate.^{34,35} Recent experiments observing that T_c is enhanced by strain³⁵⁻⁴⁰ have puzzled the relation between the van Hove singularity (VHS) and the superconductivity of Sr_2RuO_4 . Since the VHS in ruthenates lies in close vicinity to their Fermi levels, even a tiny tuning of its electronic structure may result in a drastic change by amplifying correlation-induced instability. One example of this phenomenon among the perovskite ruthenates is SrRuO_3 , with ferromagnetism arising from a high density of states (DOS) at its Fermi level due to a nearby VHS.⁴¹ To clarify the effects of the VHS in Sr_2RuO_4 , while there have been intensive studies on how the normal state reacts when the VHS approaches the Fermi level,^{21,42-45} the correlation effects across the VHS have not received much attention yet.

Pioneering studies have adequately explained the normal state properties of Sr_2RuO_4 via three-band models⁴⁶⁻⁶³ mostly employing dynamical mean-field theory (DMFT) in combination with density functional theory (DFT). Research

has shown that Hund's coupling causes orbital-dependent correlations¹³⁻¹⁵ and bad metallic behaviors at nonzero temperatures, which are prototypical features of Hund's metals. Another important local interaction in Sr_2RuO_4 is the spin-orbit coupling (SOC) that lifts the degeneracy between $j_{\text{eff}} = 1/2$ and $3/2$ ⁶⁴ (where j_{eff} is the effective total angular momentum⁶⁵) and also modifies the Fermi surface.^{25,51-54,66,67} Since the continuous-time Monte Carlo solver,⁶⁸ which has been the most widely used in this system, can hardly reach $T < 300$ K with SOC, understanding of the nonperturbative nature of electronic correlations at very low temperature is not yet satisfactory. As low temperatures can manifest a coherence of electrons and amplify the effects of the VHS lying near the Fermi level, studying the low temperature behavior of Sr_2RuO_4 with various electron configurations is expected to fill this gap and may even provide insight into its superconductivity.

In this paper, we systematically investigate how shifting the VHS affects the spin-freezing phenomena by observing single-particle responses and long-lived paramagnetic moments represented as long-time correlators via the DFT+DMFT method.^{69,70} We construct a comprehensive phase diagram to clarify the effect of Hund's coupling at various temperatures in the presence of SOC, and further investigate how the system evolves across the VHS by applying electron doping. We report a strong suppression of the Fermi liquid behavior by Hund's coupling, where the suppression is reinforced by the VHS upon doping.

II. MODEL AND METHOD

We obtain a tight-binding Hamiltonian⁷¹ of DFT-based maximally localized Wannier orbitals⁷² from the Vienna *Ab-initio* Simulation Package.⁷³ We then include the rotationally invariant Slater-Kanamori interaction⁷⁴ with a SOC of

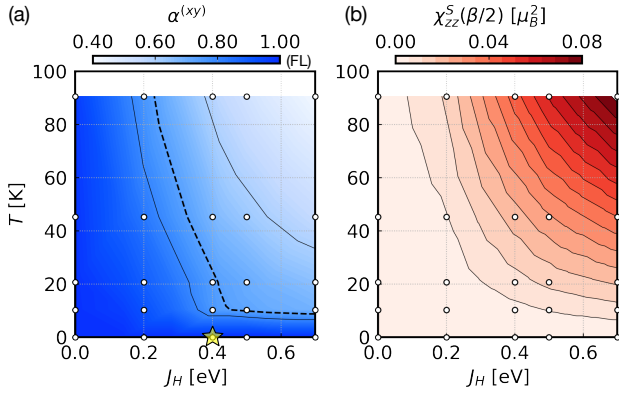


FIG. 1. (a) Power exponent α of the imaginary part of the Matsubara self-energy and (b) long-time correlator $\chi_{zz}^S(\tau = \beta/2)$ in the T - J_H plane. The dashed line in (a) denotes the crossover between Fermi liquid and Hund's metal regimes, and the yellow star marks a realistic value of J_H for Sr_2RuO_4 .

$\lambda_{\text{SOC}} = 0.1$ eV on top of the tight-binding Hamiltonian. We use an exact diagonalization (ED) solver⁷⁵ with three (six, considering spin) correlated and nine (eighteen) bath orbitals to satisfy the minimum requirement to describe multi-orbital physics.^{76–80} An advantage of the ED is that it allows us to approach zero and very low temperature in the presence of SOC without the fermionic sign problem.⁷¹ While there exist finite-size effects coming from discrete bath energy levels,^{79,81} the ED solver can provide a valuable complementary point of view inaccessible to any other impurity solver.

III. RESULTS

We first perform calculations on bare Sr_2RuO_4 to test whether the ED solver can reproduce the well-known consensus in this system. The layered structure of Sr_2RuO_4 induces a strong orbital selectivity with the aid of Hund's coupling and the VHS.^{48,61} Based on the self-energy, the d_{xy} orbital is more strongly correlated in comparison to the other two t_{2g} orbitals (see Supplementary Information for more details⁷¹). Since the d_{xy} orbital experiences a drastic change in correlations over temperature^{48,60,61} as well as Hund's coupling, its self-energy $\Sigma_{xy}(i\omega)$ is a good measure for identifying whether it follows Fermi liquid behavior or not.⁷¹ We present the power exponent of the imaginary part of the self-energies in Fig. 1(a) as Hund's coupling and temperature vary. We obtain power exponent α by fitting the self-energies to $\text{Im}\Sigma(i\omega_n) \sim \omega_n^\alpha$ with the two lowest values of ω_n . The linear power of the self-energy [marked in blue in Fig. 1(a)] with respect to the Matsubara frequency, i.e. $\text{Im}\Sigma_{xy}(i\omega) \sim \omega$, indicates that the system is in the Fermi liquid phase. This phase is stable over the entire range of temperature that we can access when Hund's coupling is zero. We define the Fermi liquid temperature T_{FL} for a given J_H as the temperature whose corresponding value of α equals the α at $T = 25$ K for $J_H = 0.4$ eV, where $T = 25$ K is based on earlier experimental works.^{26–28} To present how the Fermi liquid regime evolves as a function of J_H , we mark T_{FL}

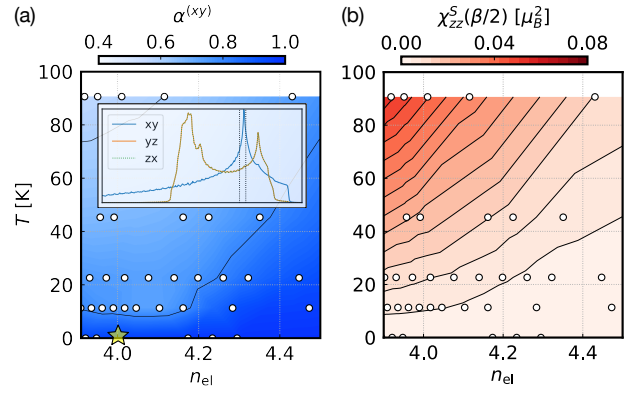


FIG. 2. Doping dependence around the van Hove singularity. (a) Power exponent of the imaginary part of the Matsubara self-energy and (b) long-time correlator $\chi_{zz}^S(\tau = \beta/2)$ in the T - n_{el} plane. Inset: Projected density of states on t_{2g} for the non-interacting case. Vertical dotted lines denote the Fermi level when $n_{\text{el}} = 4$ and 4.35 around the VHS of the d_{xy} band.

with a dashed line in Fig. 1(a). T_{FL} decreases once Hund's coupling is turned on, but the Fermi liquid ground state persists up to $J_H = 0.7$ eV. At $J_H = 0.4$ eV, which is believed to be a typical Hund's coupling strength in Sr_2RuO_4 ,^{48,53} the linear power seems to hold below 10 K in our result. This scale is comparable with previous experimental results from resistivity curves.^{26–28}

Deviation from Fermi liquid behavior has been extensively studied with three-band models, where the long-lived local magnetic moment may promote the scattering rate of electrons.^{6,78,82,83} Development of the long-lived paramagnetic moment (or so-called moment freezing) can be observed in the related magnetic susceptibility as a non-vanishing long-time correlator. The long-time correlator is defined as

$$\chi_{zz}^S(\tau = \beta/2) = \langle \hat{S}_z(\beta/2) \hat{S}_z \rangle, \quad (1)$$

where β is the inverse temperature, and \hat{S}_z is the z -component of the total angular momentum operator. To examine the origin of the power reduction in Sr_2RuO_4 , we compute the magnetic susceptibility as displayed in Fig. 1(b). We observe a clear similarity of the T - and J_H -dependencies between the two quantities in Fig. 1 (a) and (b). When the exponent indicates Fermi liquid, the long-time correlator is vanishingly small. We note here that the mere existence of the long-lived moment does not necessarily lead to time-reversal symmetry breaking; rather, the long-lived moment coexists with its time-reversal partner and the system remains paramagnetic.

We have observed that Hund's coupling suppresses the Fermi liquid regime at t_{2g}^4 , showing consistent behavior with the long-time correlator. This power exponent deviation and T_{FL} reduction in Sr_2RuO_4 are reminiscent of the J_H -induced spin-freezing crossover in the three-band model at t_{2g}^4 .^{6,7} However, there is a prominent difference upon electron doping due to the VHS of Sr_2RuO_4 . Previous model calculations for the Bethe lattice showed that Fermi liquid behavior is enhanced by electron doping on top of t_{2g}^4 ,^{6,7} while earlier

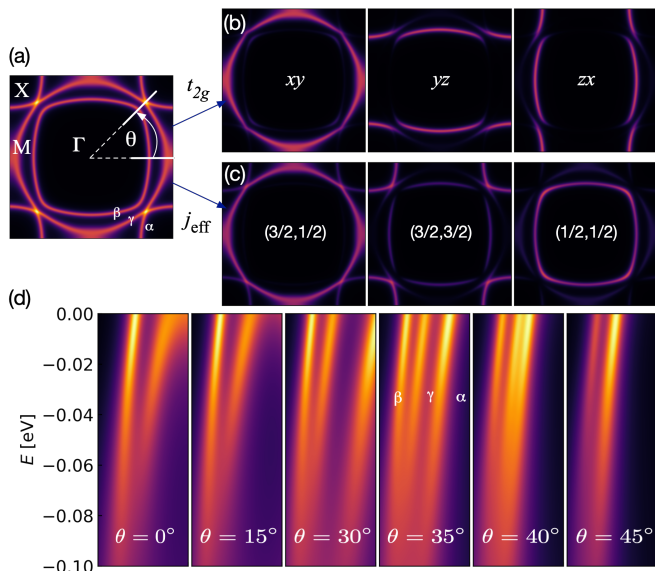


FIG. 3. Spectral density of (a) the Fermi surface and its projection onto the (b) t_{2g} - and (c) j_{eff} -basis states. (d) Dispersion along different angles θ between the ΓM and ΓX lines depicted in (a). All data are obtained with $U = 2.5$ eV, $J_H = 0.4$ eV, and $\lambda_{\text{SOC}} = 0.1$ eV at $T = 23$ K.

DFT+DMFT works focused on the Hund's metallicity of bare Sr_2RuO_4 .⁴⁸⁻⁵⁹ In Sr_2RuO_4 , though, there is a nontrivial doping dependence of the power exponent. In Fig. 2, we compare the power exponent from Σ_{xy} and the long-time correlator for electron-doped cases. Unlike the t_{2g}^4 case shown in Fig. 1, the two quantities reveal a quantitatively distinct behavior for $n_{\text{el}} > 4$ (where n_{el} is electron occupancy). Here, T_{FL} becomes minimal around $n_{\text{el}} \sim 4.1$, while the long-time correlator monotonically decreases in the regime shown in Fig. 2. This can be attributed to the electronic structure of Sr_2RuO_4 that has a VHS slightly above the Fermi level in the absence of doping.^{84,85} This supports that a mechanism separate from spin-freezing leads the power deviation. The VHS strongly suppresses hybridizations and amplifies the correlation effect delivered to the self-energy.^{48,59} The lowest T_{FL} is achieved when a Lifshitz transition appears and the VHS is expected to cross the Fermi level. Its doping concentration is, however, a bit less than one previously reported in experiments and in a non-interacting case.^{21,42} The lowest T_{FL} moves to a higher n_{el} if SOC is turned off;⁷¹ this originates from the VHS and the enhanced magnetic fluctuations by SOC, which will be discussed in more detail later.

With realistic parameters of Sr_2RuO_4 ,^{25,48} we compute the spectral functions on the Fermi level and compare them to experiments. We present the Fermi surface and low energy hole excitation spectra of Sr_2RuO_4 in Fig. 3, with parameters $U = 2.5$ eV and $J_H = 0.4$ eV. This reproduces the similar Fermi surface geometry previously obtained from ARPES spectra,^{16-23,25} which is consistent with earlier theoretical works.^{25,51,53} The strong correlation effects have an intimate connection with the Fermi surface spectra. The effective masses from our results also satisfy $m_\gamma^* > m_\beta^* > m_\alpha^*$ ⁸⁶

in good agreement with experimental results^{15,21,87} and theoretical works.^{48,49,52,53} Orbital selectivity near the Fermi level brings us the pocket-dependent scattering of three sheets, α , β , and γ , as marked in Fig. 3(a). But inside the pockets, especially β and γ , their effective masses are known to vary strongly near the ΓX line.^{25,64} This is also consistent with our spectra, as shown in Fig. 3.

Another indispensable ingredient to explain the spectral properties here is the SOC.^{53,64} While SOC is known to be essential to produce the three pockets on the Fermi surface as discussed in previous studies,^{66,67} the role of SOC in describing low-lying excitation has yet to receive much focus. As SOC introduces a mixing between t_{2g} orbitals, the strong orbital dependence of the self-energy appears controversial to underpin the importance of SOC. In spite of this, here we find that the enhanced SOC affects the character of the Fermi surface pocket from the orbital projection of the spectra.

We project the spectral weights of the Fermi level in Fig. 3(a) onto the t_{2g} and spin-orbit coupled (j_{eff}) basis states in Fig. 3(b) and (c), respectively. The two 1D-like spectra associated with the yz and zx are discontinuous near the ΓX lines due to the orbital mixing by SOC.⁶⁴ Interestingly, the Fermi pockets are well-defined on the spin-orbit eigenstates in the realistic parameter regime. The clear decomposition by the j_{eff} basis is not only limited to the Fermi level but also extends to an energy window of a few hundred meV. In Fig. 3(d), we present spectral weights as a function of energy along a few different paths between ΓM and ΓX [marked in Fig. 3(a)], which are directly related to a recent ARPES experiment.²⁵ The scattering of the γ pocket is the largest because of the strong xy components in $(j_{\text{eff}}, j_z) = (\frac{3}{2}, \pm\frac{1}{2})$. The strong j_{eff} character remains by the enhanced SOC from correlation effects. While the bare SOC is approximately 0.1 eV in Ru, the local interaction boosts the splitting induced by SOC.^{51,53,60,88,89} The effective SOC is thus twice as large as the bare value,⁵¹ which is comparable to the Hund's coupling of realistic parameters in our calculation. This indicates that the low energy excitation near the Fermi level should be described based on j_{eff} rather than on t_{2g} degrees of freedom.

Spin-orbit coupling is also vital to understand the magnetic response of this system. We compute the static susceptibility $\chi_{zz}^M(\omega = 0)$ as

$$\chi_{zz}^M(\omega) = \beta\delta(\omega) \sum_{a,b} e^{-\beta E_a} |\langle a | \hat{M}_z | b \rangle|^2 \delta(E_a - E_b) + \sum_{a,b} e^{-\beta E_a} |\langle a | \hat{M}_z | b \rangle|^2 \left(\frac{1}{\omega + \omega_{ba}} - \frac{1}{\omega - \omega_{ba}} \right), \quad (2)$$

where M is angular momentum such as S or L , summations run over the energy eigenstates, E_a is the eigenvalue of the a th energy eigenstate, and $\omega_{ba} = E_b - E_a$. The first term in Eq. (2) reflects the contribution from the long-lived moment, which is stated as the Curie term, whereas the second term expresses the Van Vleck (VV) component. Figure 4(a) displays the long-time correlator that governs the Curie term in the susceptibility. The Curie term is generated by ener-

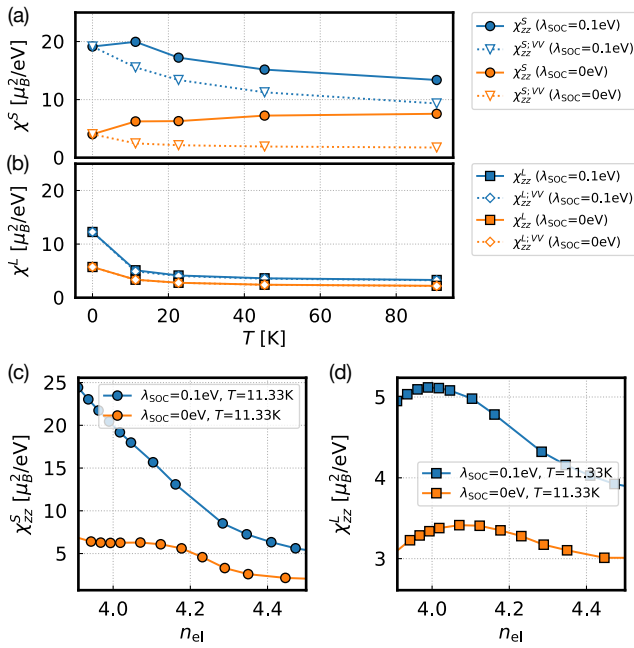


FIG. 4. Static spin susceptibilities χ_{zz}^S in the presence or absence of SOC (a) as a function of temperature for $n_{\text{el}} = 4$ and (c) as a function of n_{el} at $T = 11.33$ K. Static orbital susceptibilities χ_{zz}^L are plotted in (b) and (d). We also plot their Van Vleck contributions $\chi_{zz}^{S/L;VV}$ in (a) and (b). The data are from $(U, J_H) = (2.5, 0.4)$ eV.

getically degenerate eigenstates and directly affected by the long-lived magnetic moment. SOC lifts the degeneracy of the eigenstates and is supposed to reduce the Curie term and the long-time correlator in the Hund's metal regime ($T > T_{\text{FL}}$), as shown in Fig. 4(a). On the other hand, the degeneracy-lifting introduced by the SOC has an opposite effect on the VV term. The VV contribution comes from the angular-momentum-mediated virtual excitations between the eigenstates. The newly contributing excitations between the SOC-lifted multiplets increases the VV term, as presented in Fig. 4(b). In the range of T we consider, susceptibility is boosted by SOC due to the prominent VV contribution. This is in contrast to its effect on the single-particle response. The SOC slightly changes the self-energy, to which its renormalized masses are not very sensitive.⁶⁰ We note that the VV contribution dominates $\Delta\chi = \chi(\omega = 0) - \beta\chi(\tau = \beta/2)$, which measures the strength of fluctuations.⁹⁰ Hence, the enhanced VV at low temperature shows the significance of SOC in the correlated nature of Sr_2RuO_4 . Combined with the VHS, spin-orbit coupling makes the system reach its lowest T_{FL} at smaller n_{el} than expected when based solely on the VHS.

The temperature dependence of the two contributions of Eq. (2) shows a sharp contrast. As T increases, the long-time correlator rises while the VV counterpart decreases. Overall, the enhancement of the total susceptibility by SOC decreases as a function of T . Based on the envelope, SOC appears to suppress the susceptibility at higher temperatures. This would be consistent with a previous study that reported a reduced

spin susceptibility by SOC at $T \gtrsim 300$ K.⁵⁷

The VHS of Sr_2RuO_4 modifies its Hund's metallic behavior, as noted in the comparison to the three-band model of the Bethe lattice. Upon electron doping of t_{2g}^4 with the elliptical DOS of the Bethe lattice, the susceptibility monotonically decreases.⁹⁰ However, in Sr_2RuO_4 , the VHS manifests its singular occupancy dependence in the absence of SOC, as shown in Fig. 4(c,d). Both χ^S and χ^L show a peak near n_{el} where the Fermi level locates at the VHS, reflecting a promoted moment response due to the singularity. (Practically, the DMFT self-consistency equation recognizes the existence of the VHS by a dip in the noninteracting hybridization function.) Nonzero SOC significantly enhances the susceptibility, especially the spin responses around t_{2g}^4 [see Fig. 4(c)]. This implies the importance of SOC in detecting spin-freezing driven phenomena in theoretical calculations. Further, engineering the VHS closer to t_{2g}^4 would amplify $\chi^{S,L}$, thereby reinforcing the Hund's metallic behavior.

IV. CONCLUSIONS

In this work, we performed DFT+DMFT calculations with an exact diagonalization solver on Sr_2RuO_4 . Considering the rotationally invariant Slater-Kanamori interaction as well as spin-orbit coupling, we constructed a comprehensive phase diagram on the $T - J_H$ plane by extracting power exponents of the self-energy. The ground state is a Fermi liquid, and the system enters the Hund's metal regime as the temperature increases, with Hund's coupling suppressing the Fermi liquid temperature. We identified the particular parameter set that reproduces experimentally observed spectral functions. The ground state of Sr_2RuO_4 turned out to be very close to the Hund's metal regime in the phase diagram, reflecting its correlated nature. We then applied electron doping to study how the VHS affects the correlated metal, and found that the VHS extends the Hund's metal regime, enhancing the scattering rate of the electrons, whereas the long-time correlator weakens as the system is doped.

We also investigated the role of SOC by comparing two independent calculations, namely with and without SOC included in the DMFT loop. When SOC is included, the Fermi surface and low lying excitations are clearly decomposed in the j_{eff} basis, indicating the fundamental importance of SOC in the low energy excitation of this system. Furthermore, SOC revives the orbital degrees of freedom to affect the magnetic responses. More specifically, it reduces the long-time correlator and amplifies the VV contribution in the susceptibility. Combining these two effects, SOC increases susceptibility at sufficiently low temperature and reinforces Hund's metallicity by enhancing the magnetic fluctuations near $n_{\text{el}} = 4$. This points to the inevitability of including SOC in clarifying the roles of Hund's coupling and the VHS in Sr_2RuO_4 .

Our results call for further studies in various directions. We observed that VV susceptibility with SOC outperforms the Curie part as the temperature decreases; this reveals genuine effects of SOC in correlated multi-orbital systems. By analyzing the VHS and static susceptibility, we also showed the

importance that the electronic structure has on the correlation effects in Sr_2RuO_4 . Investigation into the interplay between the VHS and superconductivity would be another promising direction for future works. From a technical perspective, it would be interesting to test the role of additional bath orbitals by employing adaptively truncated Hilbert spaces^{81,91,92}

in highly correlated regimes where Hund's coupling is large.

ACKNOWLEDGMENTS

We thank Andrew J. Millis and Philipp Werner for insightful comments and discussion. This work was supported by the Institute for Basic Science under Grants No. IBS-R024-D1 (HJL and AG) and IBS-R009-D1 (CHK).

-
- * chkim82@snu.ac.kr
† arago@ibs.re.kr
- ¹ Kristjan Haule and Gabriel Kotliar, "Coherence–incoherence crossover in the normal state of iron oxypnictides and importance of Hund's rule coupling," *New J. Phys.* **11**, 025021 (2009).
 - ² Z P Yin, Kristjan Haule, and Gabriel Kotliar, "Kinetic frustration and the nature of the magnetic and paramagnetic states in iron pnictides and iron chalcogenides," *Nat. Mater.* **10**, 932 (2011).
 - ³ Antoine Georges, Luca de' Medici, and Jernej Mravlje, "Strong Correlations from Hund's Coupling," *Annu. Rev. Condens. Matter Phys.* **4**, 137 (2013).
 - ⁴ Luca de' Medici, Jernej Mravlje, and Antoine Georges, "Janus-Faced Influence of Hund's Rule Coupling in Strongly Correlated Materials," *Phys. Rev. Lett.* **107**, 256401 (2011).
 - ⁵ Luca de' Medici, "Hund's coupling and its key role in tuning multi-orbital correlations," *Phys. Rev. B* **83**, 205112 (2011).
 - ⁶ Philipp Werner, Emanuel Gull, Matthias Troyer, and Andrew J Millis, "Spin Freezing Transition and Non-Fermi-Liquid Self-Energy in a Three-Orbital Model," *Phys. Rev. Lett.* **101**, 166405 (2008).
 - ⁷ Aaram J Kim, Harald O Jeschke, Philipp Werner, and Roser Valentí, "J Freezing and Hund's Rules in Spin-Orbit-Coupled Multi-orbital Hubbard Models," *Phys. Rev. Lett.* **118**, 086401 (2017).
 - ⁸ Akihisa Koga, Norio Kawakami, T M Rice, and Manfred Sgrist, "Orbital-Selective Mott Transitions in the Degenerate Hubbard Model," *Phys. Rev. Lett.* **92**, 216402 (2004); V I Anisimov, I A Nekrasov, D E Kondakov, T M Rice, and M Sgrist, "Orbital-selective Mott-insulator transition in $\text{Ca}_{2-x}\text{Sr}_x\text{RuO}_4$," *Eur. Phys. J. B* **25**, 191–201 (2002).
 - ⁹ Philipp Werner and Andrew J Millis, "High-Spin to Low-Spin and Orbital Polarization Transitions in Multi-orbital Mott Systems," *Phys. Rev. Lett.* **99**, 126405 (2007).
 - ¹⁰ Philipp Werner, Emanuel Gull, and Andrew J Millis, "Metal-insulator phase diagram and orbital selectivity in three-orbital models with rotationally invariant Hund coupling," *Phys. Rev. B* **79**, 115119 (2009).
 - ¹¹ Luca de' Medici, S R Hassan, Massimo Capone, and Xi Dai, "Orbital-Selective Mott Transition out of Band Degeneracy Lifting," *Phys. Rev. Lett.* **102**, 126401 (2009).
 - ¹² Philipp Werner, Shintaro Hoshino, and Hiroshi Shinaoka, "Spin-freezing perspective on cuprates," *Phys. Rev. B* **94**, 245134 (2016).
 - ¹³ A P Mackenzie, S R Julian, A J Diver, G J McMullan, M P Ray, G G Lonzarich, Y Maeno, S Nishizaki, and T Fujita, "Quantum Oscillations in the Layered Perovskite Superconductor Sr_2RuO_4 ," *Phys. Rev. Lett.* **76**, 3786–3789 (1996).
 - ¹⁴ C Bergemann, S R Julian, A P Mackenzie, S NishiZaki, and Y Maeno, "Detailed Topography of the Fermi Surface of Sr_2RuO_4 ," *Phys. Rev. Lett.* **84**, 2662–2665 (2000).
 - ¹⁵ C. Bergemann, A. P. Mackenzie, S. R. Julian, D. Forsythe, and E. Ohmichi, "Quasi-two-dimensional Fermi liquid properties of the unconventional superconductor Sr_2RuO_4 ," *Adv. Phys.* **52**, 639–725 (2003).
 - ¹⁶ A Damascelli, D H Lu, K M Shen, N P Armitage, F Ronning, D L Feng, C Kim, Z.-X. Shen, T Kimura, Y Tokura, Z Q Mao, and Y Maeno, "Fermi Surface, Surface States, and Surface Reconstruction in Sr_2RuO_4 ," *Phys. Rev. Lett.* **85**, 5194–5197 (2000).
 - ¹⁷ K M Shen, A Damascelli, D H Lu, N P Armitage, F Ronning, D L Feng, C Kim, Z.-X. Shen, D J Singh, I I Mazin, S Nakatsuji, Z Q Mao, Y Maeno, T Kimura, and Y Tokura, "Surface electronic structure of Sr_2RuO_4 ," *Phys. Rev. B* **64**, 180502(R) (2001).
 - ¹⁸ H Iwasawa, Y Aiura, T Saitoh, I Hase, S I Ikeda, Y Yoshida, H Bando, M Higashiguchi, Y Miura, X Y Cui, K Shimada, H Namatame, and M Taniguchi, "Orbital selectivity of the kink in the dispersion of Sr_2RuO_4 ," *Phys. Rev. B* **72**, 104514 (2005).
 - ¹⁹ N J C Ingle, K M Shen, F Baumberger, W Meevasana, D H Lu, Z.-X. Shen, A Damascelli, S Nakatsuji, Z Q Mao, Y Maeno, T Kimura, and Y Tokura, "Quantitative analysis of Sr_2RuO_4 angle-resolved photoemission spectra: Many-body interactions in a model Fermi liquid," *Phys. Rev. B* **72**, 205114 (2005).
 - ²⁰ T E Kidd, T Valla, A V Fedorov, P D Johnson, R J Cava, and M K Haas, "Orbital Dependence of the Fermi Liquid State in Sr_2RuO_4 ," *Phys. Rev. Lett.* **94**, 107003 (2005).
 - ²¹ K M Shen, N Kikugawa, C Bergemann, L Balicas, F Baumberger, W Meevasana, N J C Ingle, Y Maeno, Z.-X. Shen, and A P Mackenzie, "Evolution of the Fermi Surface and Quasiparticle Renormalization through a van Hove Singularity in $\text{Sr}_{2-y}\text{La}_y\text{RuO}_4$," *Phys. Rev. Lett.* **99**, 187001 (2007).
 - ²² H Iwasawa, Y Yoshida, I Hase, S Koikegami, H Hayashi, J Jiang, K Shimada, H Namatame, M Taniguchi, and Y Aiura, "Interplay among Coulomb Interaction, Spin-Orbit Interaction, and Multiple Electron-Boson Interactions in Sr_2RuO_4 ," *Phys. Rev. Lett.* **105**, 226406 (2010).
 - ²³ H Iwasawa, Y Yoshida, I Hase, K Shimada, H Namatame, M Taniguchi, and Y Aiura, "High-Energy Anomaly in the Band Dispersion of the Ruthenate Superconductor," *Phys. Rev. Lett.* **109**, 066404 (2012).
 - ²⁴ D Stricker, J Mravlje, C Berthod, R Fittipaldi, A Vecchione, A Georges, and D van der Marel, "Optical Response of Sr_2RuO_4 Reveals Universal Fermi-Liquid Scaling and Quasiparticles Beyond Landau Theory," *Phys. Rev. Lett.* **113**, 087404 (2014).
 - ²⁵ A. Tamai, M. Zingl, E. Rozbicki, E. Cappelli, S. Riccò, A. de la Torre, S. McKeown Walker, F. Y. Bruno, P. D. C. King, W. Meevasana, M. Shi, M. Radović, N. C. Plumb, A. S. Gibbs, A. P. Mackenzie, C. Berthod, H. U. R. Strand, M. Kim, A. Georges, and F. Baumberger, "High-Resolution Photoemission on Sr_2RuO_4 Reveals Correlation-Enhanced Effective Spin-Orbit Coupling and Dominantly Local Self-Energies," *Phys. Rev. X* **9**, 021048 (2019).
 - ²⁶ Yoshiteru Maeno, Koji Yoshida, Hiroaki Hashimoto, Shuji

- Nishizaki, Shin-ichi Ikeda, Minoru Nohara, Toshizo Fujita, Andrew P. Mackenzie, Nigel E. Hussey, J. Georg Bednorz, and Frank Lichtenberg, “Two-Dimensional Fermi Liquid Behavior of the Superconductor Sr_2RuO_4 ,” *J. Phys. Soc. Japan* **66**, 1405–1408 (1997).
- ²⁷ N E Hussey, A P Mackenzie, J R Cooper, Y Maeno, S Nishizaki, and T Fujita, “Normal-state magnetoresistance of Sr_2RuO_4 ,” *Phys. Rev. B* **57**, 5505 (1998).
- ²⁸ A W Tyler, A P Mackenzie, S NishiZaki, and Y Maeno, “High-temperature resistivity of Sr_2RuO_4 : Bad metallic transport in a good metal,” *Phys. Rev. B* **58**, R10107(R) (1998).
- ²⁹ Y Maeno, H Hashimoto, K Yoshida, S Nishizaki, T Fujita, J G Bednorz, and F Lichtenberg, “Superconductivity in a layered perovskite without copper,” *Nature* **372**, 532–534 (1994).
- ³⁰ T M Rice and M Sigrist, “ Sr_2RuO_4 : an electronic analogue of ^3He ?” *J. Phys. Condens. Matter* **7**, L643–L648 (1995).
- ³¹ A P Mackenzie, R K W Haselwimmer, A W Tyler, G G Lonzarich, Y Mori, S Nishizaki, and Y Maeno, “Extremely Strong Dependence of Superconductivity on Disorder in Sr_2RuO_4 ,” *Phys. Rev. Lett.* **80**, 161–164 (1998).
- ³² K Ishida, H Mukuda, Y Kitaoka, K Asayama, Z Q Mao, Y Mori, and Y Maeno, “Spin-triplet superconductivity in Sr_2RuO_4 identified by ^{17}O Knight shift,” *Nature* **396**, 658–660 (1998).
- ³³ Andrew Peter Mackenzie and Yoshiteru Maeno, “The superconductivity of Sr_2RuO_4 and the physics of spin-triplet pairing,” *Rev. Mod. Phys.* **75**, 657–712 (2003).
- ³⁴ Andrew P Mackenzie, Thomas Scaffidi, Clifford W Hicks, and Yoshiteru Maeno, “Even odder after twenty-three years: the superconducting order parameter puzzle of Sr_2RuO_4 ,” *npj Quantum Mater.* **2**, 40 (2017).
- ³⁵ A Pustogow, Yongkang Luo, A Chronister, Y.-S. Su, D A Sokolov, F Jerzembeck, A P Mackenzie, C W Hicks, N Kikugawa, S Raghu, E D Bauer, and S E Brown, “Constraints on the superconducting order parameter in Sr_2RuO_4 from oxygen-17 nuclear magnetic resonance,” *Nature* **574**, 72–75 (2019).
- ³⁶ Clifford W Hicks, Daniel O Brodsky, Edward A Yelland, Alexandra S Gibbs, Jan A N Bruin, Mark E Barber, Stephen D Edkins, Keigo Nishimura, Shingo Yonezawa, Yoshiteru Maeno, and Andrew P Mackenzie, “Strong Increase of T_c of Sr_2RuO_4 Under Both Tensile and Compressive Strain,” *Science* **344**, 283 (2014).
- ³⁷ Alexander Steppke, Lishan Zhao, Mark E Barber, Thomas Scaffidi, Fabian Jerzembeck, Helge Rosner, Alexandra S Gibbs, Yoshiteru Maeno, Steven H Simon, Andrew P Mackenzie, and Clifford W Hicks, “Strong peak in T_c of Sr_2RuO_4 under uniaxial pressure,” *Science* **355**, eaaf9398 (2017).
- ³⁸ M. E. Barber, A. S. Gibbs, Y Maeno, A. P. Mackenzie, and C. W. Hicks, “Resistivity in the Vicinity of a van Hove Singularity: Sr_2RuO_4 under Uniaxial Pressure,” *Phys. Rev. Lett.* **120**, 076602 (2018).
- ³⁹ Yongkang Luo, A. Pustogow, P. Guzman, A. P. Dioguardi, S. M. Thomas, F. Ronning, N. Kikugawa, D. A. Sokolov, F. Jerzembeck, A. P. Mackenzie, C. W. Hicks, E. D. Bauer, I. I. Mazin, and S. E. Brown, “Normal State ^{17}O NMR Studies of Sr_2RuO_4 under Uniaxial Stress,” *Phys. Rev. X* **9**, 021044 (2019).
- ⁴⁰ Mark E Barber, Frank Lechermann, Sergey V Streltsov, Sergey L Skornyakov, Sayak Ghosh, B J Ramshaw, Naoki Kikugawa, Dmitry A Sokolov, Andrew P Mackenzie, Clifford W Hicks, and I I Mazin, “Role of correlations in determining the Van Hove strain in Sr_2RuO_4 ,” *Phys. Rev. B* **100**, 245139 (2019).
- ⁴¹ Qiang Han, Hung T Dang, and A J Millis, “Ferromagnetism and correlation strength in cubic barium ruthenate in comparison to strontium and calcium ruthenate: A dynamical mean-field study,” *Phys. Rev. B* **93**, 155103 (2016).
- ⁴² N Kikugawa, A P Mackenzie, C Bergemann, R A Borzi, S A Grigera, and Y Maeno, “Rigid-band shift of the Fermi level in the strongly correlated metal: $\text{Sr}_{2-y}\text{La}_y\text{RuO}_4$,” *Phys. Rev. B* **70**, 060508(R) (2004).
- ⁴³ Naoki Kikugawa, Christoph Bergemann, Andrew Peter Mackenzie, and Yoshiteru Maeno, “Band-selective modification of the magnetic fluctuations in Sr_2RuO_4 : A study of substitution effects,” *Phys. Rev. B* **70**, 134520 (2004).
- ⁴⁴ B Burganov, C Adamo, A Mulder, M Uchida, P. D. C. King, J. W. Harter, D. E. Shai, A. S. Gibbs, A. P. Mackenzie, R Uecker, M Bruetzam, M. R. Beasley, C. J. Fennie, D. G. Schlom, and K. M. Shen, “Strain Control of Fermiology and Many-Body Interactions in Two-Dimensional Ruthenates,” *Phys. Rev. Lett.* **116**, 197003 (2016).
- ⁴⁵ František Herman, Jonathan Buhmann, Mark H Fischer, and Manfred Sigrist, “Deviation from Fermi-liquid transport behavior in the vicinity of a Van Hove singularity,” *Phys. Rev. B* **99**, 184107 (2019).
- ⁴⁶ A Liebsch and A Lichtenstein, “Photoemission Quasiparticle Spectra of Sr_2RuO_4 ,” *Phys. Rev. Lett.* **84**, 1591–1594 (2000).
- ⁴⁷ Z V Pchelkina, I A Nekrasov, Th. Pruschke, A Sekiyama, S Suga, V I Anisimov, and D Vollhardt, “Evidence for strong electronic correlations in the spectra of Sr_2RuO_4 ,” *Phys. Rev. B* **75**, 35122 (2007).
- ⁴⁸ Jernej Mravlje, Markus Aichhorn, Takashi Miyake, Kristjan Haule, Gabriel Kotliar, and Antoine Georges, “Coherence-Incoherence Crossover and the Mass-Renormalization Puzzles in Sr_2RuO_4 ,” *Phys. Rev. Lett.* **106**, 096401 (2011).
- ⁴⁹ Xiaoyu Deng, Kristjan Haule, and Gabriel Kotliar, “Transport Properties of Metallic Ruthenates: A DFT + DMFT Investigation,” *Phys. Rev. Lett.* **116**, 256401 (2016).
- ⁵⁰ Jernej Mravlje and Antoine Georges, “Thermopower and Entropy: Lessons from Sr_2RuO_4 ,” *Phys. Rev. Lett.* **117**, 036401 (2016).
- ⁵¹ Guoren Zhang, Evgeny Gorelov, Esmaeel Sarvestani, and Eva Pavarini, “Fermi Surface of Sr_2RuO_4 : Spin-Orbit and Anisotropic Coulomb Interaction Effects,” *Phys. Rev. Lett.* **116**, 106402 (2016).
- ⁵² Esmaeel Sarvestani, Gouren Zhang, Evgeny Gorelov, and Eva Pavarini, “Effective masses, lifetimes, and optical conductivity in Sr_2RuO_4 and $\text{Sr}_3\text{Ru}_2\text{O}_7$: Interplay of spin-orbit, crystal-field, and Coulomb tetragonal tensor interactions,” *Phys. Rev. B* **97**, 085141 (2018).
- ⁵³ Minjae Kim, Jernej Mravlje, Michel Ferrero, Olivier Parcollet, and Antoine Georges, “Spin-Orbit Coupling and Electronic Correlations in Sr_2RuO_4 ,” *Phys. Rev. Lett.* **120**, 126401 (2018).
- ⁵⁴ Jorge I Facio, Jernej Mravlje, Leonid Pourovskii, Pablo S Cornaglia, and V Vildosola, “Spin-orbit and anisotropic strain effects on the electronic correlations in Sr_2RuO_4 ,” *Phys. Rev. B* **98**, 085121 (2018).
- ⁵⁵ Xiaoyu Deng, Katharina M Stadler, Kristjan Haule, Andreas Weichselbaum, Jan von Delft, and Gabriel Kotliar, “Signatures of Mottness and Hundness in archetypal correlated metals,” *Nat. Commun.* **10**, 2721 (2019).
- ⁵⁶ Manuel Zingl, Jernej Mravlje, Markus Aichhorn, Olivier Parcollet, and Antoine Georges, “Hall coefficient signals orbital differentiation in the Hund’s metal Sr_2RuO_4 ,” *npj Quantum Mater.* **4**, 35 (2019).
- ⁵⁷ Hugo U R Strand, Manuel Zingl, Nils Wentzell, Olivier Parcollet, and Antoine Georges, “Magnetic response of Sr_2RuO_4 : Quasi-local spin fluctuations due to Hund’s coupling,” *Phys. Rev. B* **100**, 125120 (2019).
- ⁵⁸ O Gingras, R Nourafkan, A.-M. S Tremblay, and M Côté, “Superconducting Symmetries of Sr_2RuO_4 from First-Principles Electronic Structure,” *Phys. Rev. Lett.* **123**, 217005 (2019).
- ⁵⁹ Fabian B Kugler, Manuel Zingl, Hugo U R Strand, Seung-Sup B

- Lee, Jan von Delft, and Antoine Georges, “Strongly Correlated Materials from a Numerical Renormalization Group Perspective: How the Fermi-Liquid State of Sr_2RuO_4 Emerges,” *Phys. Rev. Lett.* **124**, 16401 (2020).
- ⁶⁰ Nils-Oliver Linden, Manuel Zingl, Claudius Hubig, Olivier Parcollet, and Ulrich Schollwöck, “Imaginary-time matrix product state impurity solver in a real material calculation: Spin-orbit coupling in Sr_2RuO_4 ,” *Phys. Rev. B* **101**, 41101 (2020).
- ⁶¹ Jonathan Karp, Max Bramberger, Martin Grundner, Ulrich Schollwöck, Andrew J. Millis, and Manuel Zingl, “ Sr_2MoO_4 and Sr_2RuO_4 : Disentangling the Roles of Hund’s and van Hove Physics,” (2020), arXiv:2004.12515.
- ⁶² Siheon Ryee, Seung Woo Jang, Hiori Kino, Takao Kotani, and Myung Joon Han, “Quasiparticle self-consistent GW calculation of Sr_2RuO_4 and SrRuO_3 ,” *Phys. Rev. B* **93**, 075125 (2016).
- ⁶³ Sergio Cobo, Felix Ahn, Ilya Eremin, and Alireza Akbari, “Anisotropic spin fluctuations in Sr_2RuO_4 : Role of spin-orbit coupling and induced strain,” *Phys. Rev. B* **94**, 224507 (2016).
- ⁶⁴ C. N. Veenstra, Z.-H. Zhu, M Raichle, B. M. Ludbrook, A Nicolaou, B Slomski, G Landolt, S Kittaka, Y Maeno, J. H. Dil, I. S. Elfimov, M. W. Haverkort, and A Damascelli, “Spin-Orbital Entanglement and the Breakdown of Singlets and Triplets in Sr_2RuO_4 Revealed by Spin- and Angle-Resolved Photoemission Spectroscopy,” *Phys. Rev. Lett.* **112**, 127002 (2014).
- ⁶⁵ B J Kim, Hosub Jin, S J Moon, J.-Y. Kim, B.-G. Park, C S Leem, Jaejun Yu, T W Noh, C Kim, S.-J. Oh, J.-H. Park, V Durairaj, G Cao, and E Rotenberg, “Novel $J_{\text{eff}} = 1/2$ Mott State Induced by Relativistic Spin-Orbit Coupling in Sr_2IrO_4 ,” *Phys. Rev. Lett.* **101**, 76402 (2008).
- ⁶⁶ E Pavarini and I. I. Mazin, “First-principles study of spin-orbit effects and NMR in Sr_2RuO_4 ,” *Phys. Rev. B* **74**, 035115 (2006).
- ⁶⁷ M W Haverkort, I S Elfimov, L H Tjeng, G A Sawatzky, and A Damascelli, “Strong spin-orbit coupling effects on the fermi surface of Sr_2RuO_4 and Sr_2RhO_4 ,” *Phys. Rev. Lett.* **101**, 026406 (2008).
- ⁶⁸ Emanuel Gull, Andrew J Millis, Alexander I Lichtenstein, Alexey N Rubtsov, Matthias Troyer, and Philipp Werner, “Continuous-time Monte Carlo methods for quantum impurity models,” *Rev. Mod. Phys.* **83**, 349–404 (2011).
- ⁶⁹ Antoine Georges, G Kotliar, Werner Krauth, and M J Rozenberg, “Dynamical mean-field theory of strongly correlated fermion systems and the limit of infinite dimensions,” *Rev. Mod. Phys.* **68**, 13–125 (1996).
- ⁷⁰ G. Kotliar, S. Savrasov, K. Haule, V. Oudovenko, O. Parcollet, and C. Marianetti, “Electronic structure calculations with dynamical mean-field theory,” *Rev. Mod. Phys.* **78**, 865–951 (2006).
- ⁷¹ See Supplementary Information for more details.
- ⁷² Arash A Mostofi, Jonathan R Yates, Giovanni Pizzi, Young-Su Lee, Ivo Souza, David Vanderbilt, and Nicola Marzari, “An updated version of wannier90: A tool for obtaining maximally-localised Wannier functions,” *Comput. Phys. Commun.* **185**, 2309–2310 (2014).
- ⁷³ G Kresse and D Joubert, “From ultrasoft pseudopotentials to the projector augmented-wave method,” *Phys. Rev. B* **59**, 1758–1775 (1999).
- ⁷⁴ Junjiro Kanamori, “Electron Correlation and Ferromagnetism of Transition Metals,” *Prog. Theor. Phys.* **30**, 275–289 (1963).
- ⁷⁵ Michel Caffarel and Werner Krauth, “Exact diagonalization approach to correlated fermions in infinite dimensions: Mott transition and superconductivity,” *Phys. Rev. Lett.* **72**, 1545–1548 (1994).
- ⁷⁶ Erik Koch, Giorgio Sangiovanni, and Olle Gunnarsson, “Sum rules and bath parametrization for quantum cluster theories,” *Phys. Rev. B* **78**, 115102 (2008).
- ⁷⁷ David Sénéchal, “Bath optimization in the cellular dynamical mean-field theory,” *Phys. Rev. B* **81**, 235125 (2010).
- ⁷⁸ Ansgar Liebsch and Hiroshi Ishida, “Temperature and bath size in exact diagonalization dynamical mean field theory,” *J. Phys. Condens. Matter* **24**, 53201 (2012).
- ⁷⁹ Ara Go and Andrew J Millis, “Spatial Correlations and the Insulating Phase of the High- T_c Cuprates: Insights from a Configuration-Interaction-Based Solver for Dynamical Mean Field Theory,” *Phys. Rev. Lett.* **114**, 016402 (2015).
- ⁸⁰ Edoardo Fertitta and George H Booth, “Rigorous wave function embedding with dynamical fluctuations,” *Phys. Rev. B* **98**, 235132 (2018).
- ⁸¹ Ara Go and Andrew J Millis, “Adaptively truncated Hilbert space based impurity solver for dynamical mean-field theory,” *Phys. Rev. B* **96**, 085139 (2017).
- ⁸² K. M. Stadler, Z. P. Yin, J von Delft, G Kotliar, and A Weichselbaum, “Dynamical Mean-Field Theory Plus Numerical Renormalization-Group Study of Spin-Orbital Separation in a Three-Band Hund Metal,” *Phys. Rev. Lett.* **115**, 136401 (2015).
- ⁸³ Alexander Kowalski, Andreas Hausoel, Markus Wallerberger, Patrik Gunacker, and Giorgio Sangiovanni, “State and superstate sampling in hybridization-expansion continuous-time quantum Monte Carlo,” *Phys. Rev. B* **99**, 155112 (2019).
- ⁸⁴ Tamio Oguchi, “Electronic band structure of the superconductor Sr_2RuO_4 ,” *Phys. Rev. B* **51**, 1385–1388 (1995).
- ⁸⁵ David J Singh, “Relationship of Sr_2RuO_4 to the superconducting layered cuprates,” *Phys. Rev. B* **52**, 1358–1361 (1995).
- ⁸⁶ We obtain $(m_{(\frac{3}{2}, \frac{1}{2})}^*, m_{(\frac{1}{2}, \frac{1}{2})}^*, m_{(\frac{3}{2}, \frac{3}{2})}^*) \simeq (5.60, 5.09, 3.94)$ at $T = 0$ K and $(4.56, 4.27, 3.61)$ at $T = 11$ K. We use a fourth order polynomial with lowest six Matsubara frequencies and fit imaginary part of self-energy. See Supplementary Information for more details.
- ⁸⁷ Takeshi Kondo, M Ochi, M Nakayama, H Taniguchi, S Akebi, K Kuroda, M Arita, S Sakai, H Namatame, M Taniguchi, Y Maeno, R Arita, and S Shin, “Orbital-Dependent Band Narrowing Revealed in an Extremely Correlated Hund’s Metal Emerging on the Topmost Layer of Sr_2RuO_4 ,” *Phys. Rev. Lett.* **117**, 247001 (2016).
- ⁸⁸ Guo-Qiang Liu, V N Antonov, O Jepsen, and O K Andersen., “Coulomb-Enhanced Spin-Orbit Splitting: The Missing Piece in the Sr_2RhO_4 Puzzle,” *Phys. Rev. Lett.* **101**, 26408 (2008).
- ⁸⁹ Jörg Bünemann, Thorben Linneweber, Ute Löw, Frithjof B Anders, and Florian Gebhard, “Interplay of Coulomb interaction and spin-orbit coupling,” *Phys. Rev. B* **94**, 035116 (2016).
- ⁹⁰ Shintaro Hoshino and Philipp Werner, “Superconductivity from Emerging Magnetic Moments,” *Phys. Rev. Lett.* **115**, 247001 (2015).
- ⁹¹ Dominika Zgid and Garnet Kin-Lic Chan, “Dynamical mean-field theory from a quantum chemical perspective,” *J. Chem. Phys.* **134**, 94115 (2011).
- ⁹² Y Lu, M Höppner, O Gunnarsson, and M W Haverkort, “Efficient real-frequency solver for dynamical mean-field theory,” *Phys. Rev. B* **90**, 085102 (2014).

Supplemental Material for “Fermi liquid behavior and van Hove singularity in Sr₂RuO₄”

Hyeong Jun Lee,^{1,2,3} Choong H. Kim,^{2,3,*} and Ara Go^{1,†}

¹Center for Theoretical Physics of Complex Systems, Institute for Basic Science (IBS), Daejeon 34126, Republic of Korea

²Center for Correlated Electron Systems, Institute for Basic Science (IBS), Seoul 08826, Republic of Korea

³Department of Physics and Astronomy, Seoul National University, Seoul 08826, Republic of Korea

Tight-binding Hamiltonian

We obtain the tight-binding (TB) Hamiltonian $\mathcal{H}_{\text{TB}} = \sum_{i,j} \sum_{\mu,\beta} t_{\mu\nu}^{ij} c_{i\mu}^\dagger c_{j\nu}$ on the maximally localized Wannier functions (MLWF) from density functional theory (DFT) calculation with the PBEsol functional. The indices μ and ν denote the t_{2g} orbitals. Some parameters between nearest neighbors and next-nearest neighbors are obtained as $t_{xy,xy}^{\pm 1,0,0} = -0.388$, $t_{yz,yz}^{\pm 1,0,0} = -0.325$, $t_{yz,yz}^{0,\pm 1,0} = -0.048$, $t_{xy,xy}^{\pm 1,\pm 1,0} = -0.130$, $t_{yz,yz}^{\pm 1,\pm 1,0} = -0.017$, and $t_{xy,yz}^{\pm 1,\pm 1,0} = 0.010$. We introduce spin-orbit coupling (SOC) with $\lambda_{\text{SOC}} \sum_i \mathbf{l}_i \cdot \mathbf{s}_i$, where i is the index for electrons on a site, in the TB Hamiltonian. From fitting the band structure of the Wannier to the DFT bands having SOC, the strength of the SOC, λ_{SOC} , is set to 0.1 eV (as shown in Fig. S1). We perform dynamical mean-field theory (DMFT) calculation based on the top of this TB Hamiltonian with j_{eff} -basis states.

We also perform local-density approximation (LDA) calculations to obtain the MLWF and TB Hamiltonian. With slightly reduced bandwidths compared to that from PBEsol, this gives only a minor correction on the magnitudes of the self-energies for fixed U and J_H of our interest in the DMFT calculation. We confirm that this correction does not significantly affect our main result; it is expected to lead to a small shift in the critical Hund’s coupling strength associated with the resulting correlation effects.

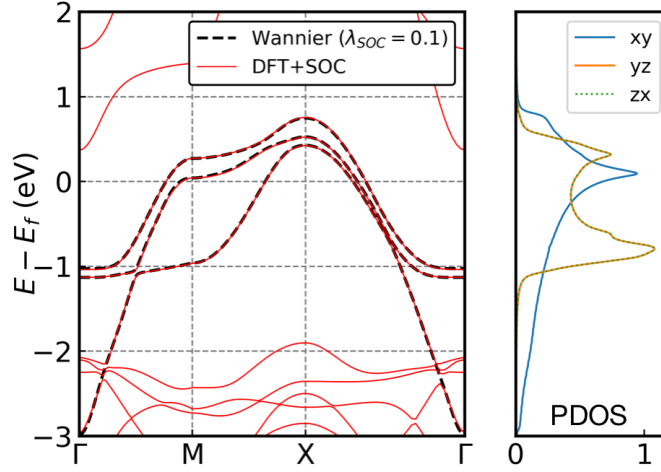


FIG. S1. (a) DFT and MLWF bands of Sr₂RuO₄ along the high-symmetry lines. (b) Density of states of MLWF bands on t_{2g} .

Orbital-dependent correlations

From the DFT band structure and density of states, the effective model of Sr₂RuO₄ can be described by two degenerate d_{yz} and d_{zx} bands along with the other d_{xy} band. This difference between the bands enables Sr₂RuO₄ to gain orbital selectivity, which is one of the remarkable aspects of the correlation effects driven by Hund’s coupling. Figure S2(a) shows the orbital-dependent correlations in the self-energy on t_{2g} . The imaginary part of the self-energy of the d_{xy} band is more enhanced than that of d_{yz}/d_{zx} near $\omega = 0$. This difference exists noticeably in low-energy excitations and maintains up to 0.5 eV.

The Matsubara-frequency self-energy near $\omega = 0$ is associated with renormalized mass and a renormalization factor when its imaginary part follows linear (or Fermi liquid) behavior in ω_n . From the $T = 0$ data, we compute and compare the renormalized masses m^* on t_{2g} and j_{eff} defined as $m^* = (1 - \partial_\omega \text{Im}\Sigma(i\omega)|_{\omega \rightarrow 0})^{-1}$. We obtain $(m_{(\frac{3}{2}, \frac{1}{2})}^*, m_{(\frac{1}{2}, \frac{1}{2})}^*, m_{(\frac{3}{2}, \frac{3}{2})}^*) \simeq (5.60, 5.09, 3.94)$ at $T = 0$ K and $(4.56, 4.27, 3.61)$ at $T = 11$ K. We use a fourth order polynomial with the lowest six Matsubara frequencies and

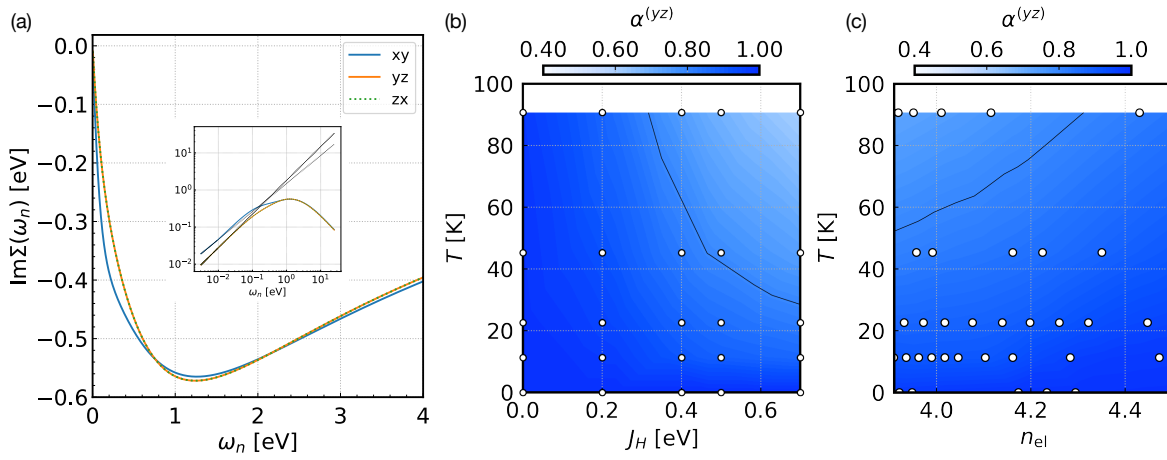


FIG. S2. (a) Imaginary part of the Matsubara self-energy projected on the t_{2g} -basis in Sr_2RuO_4 at $T \simeq 10$ K. The inset is a log-log plot with fitting lines showing different power exponents: -0.75 for d_{xy} and 0.91 for d_{yz}/d_{zx} . (b,c) Power exponent α of the d_{yz} component in the T - J_H plane (b) and in the T - n plane (c).

fit the imaginary part of self-energy; comparisons to m^* from an experiment and previous DMFT studies with the t_{2g} and j_{eff} basis are given in Table S1.

TABLE S1. Renormalized masses on the t_{2g} and j_{eff} basis at various temperatures compared to previous Sr_2RuO_4 studies.

	m_{xy}	$m_{yz/zx}$	Etc.
	$(m_{(\frac{3}{2}, \frac{1}{2})})$	$(m_{(\frac{1}{2}, \frac{1}{2})})$	$(m_{(\frac{3}{2}, \frac{3}{2})})$
Mravlje <i>et al.</i> 2011PRL [S1]	4.5	3.3	imag. freq. $T \gtrsim 50$ K
Kim <i>et al.</i> 2018PRL [S2]	4.0	3.1	real freq. $T = 230$ K ($\lambda_{\text{SOC}} = 0.1$ eV)
Tamai <i>et al.</i> 2019PRX [S3]	5.55(30)	3.33(30)	real freq. $T = 29$ K
Kugler <i>et al.</i> 2020PRL [S4]	~ 5.9	~ 3.6	real freq. (saturating below 10 K or 40 K)
Linden <i>et al.</i> 2020PRB [S5]	5.26	3.45	imag. freq. (probably at $T = 58$ K)
	5.00	3.70	imag. freq. (probably at $T = 58$ K, $\lambda_{\text{SOC}} = 0.1$ eV)
Karp <i>et al.</i> 2020arXiv [S6]	~ 5.3	~ 3.4	imag. freq. at 0 K, MPS ($\beta^{\text{fit}} = 200 \text{ eV}^{-1}$)
	~ 5.0	~ 3.5	imag. freq. at 29 K, CTHYB
Ours	4.86	3.50	imag. freq. at 0 K (t_{2g} , $\beta^{\text{fit}} = 256 \text{ eV}^{-1}$)
($\lambda_{\text{SOC}} = 0$ eV)	6.51	3.82	imag. freq. at 0 K (t_{2g} , $\beta^{\text{fit}} \rightarrow \infty$)
	5.38	3.63	imag. freq. at 11 K (t_{2g})
	4.76	3.48	imag. freq. at 23 K (t_{2g})
Ours	6.69	4.04	imag. freq. at 0 K (t_{2g})
($\lambda_{\text{SOC}} = 0.1$ eV)	5.03	3.67	imag. freq. at 11 K (t_{2g})
	5.60	5.09	3.94
	4.56	4.27	3.61
			imag. freq. at 11 K (j_{eff})
Experiment (dHvA) [S7]	5.5	3.5	3.0
			$(m_\gamma, m_\beta, m_\alpha)$

Self-energy with electron-doping and power exponent α

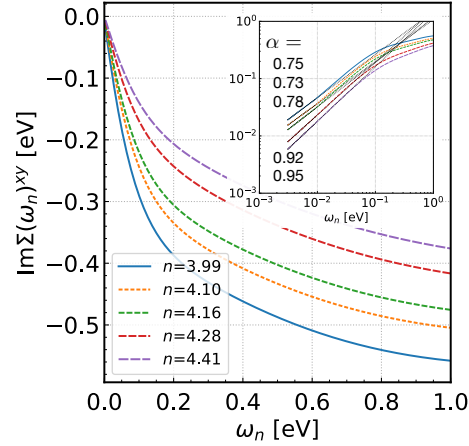


FIG. S3. Imaginary part of the self-energies in the Matsubara frequencies for various electron occupations with $(U, J_H, \lambda_{\text{SOC}}) = (2.5, 0.4, 0.1)$ eV at $T = 11$ K. The inset is a log-log plot of the same data, their fitting lines of $(\omega_n)^\alpha$, and their corresponding α values.

Comparison to the case in the absence of SOC

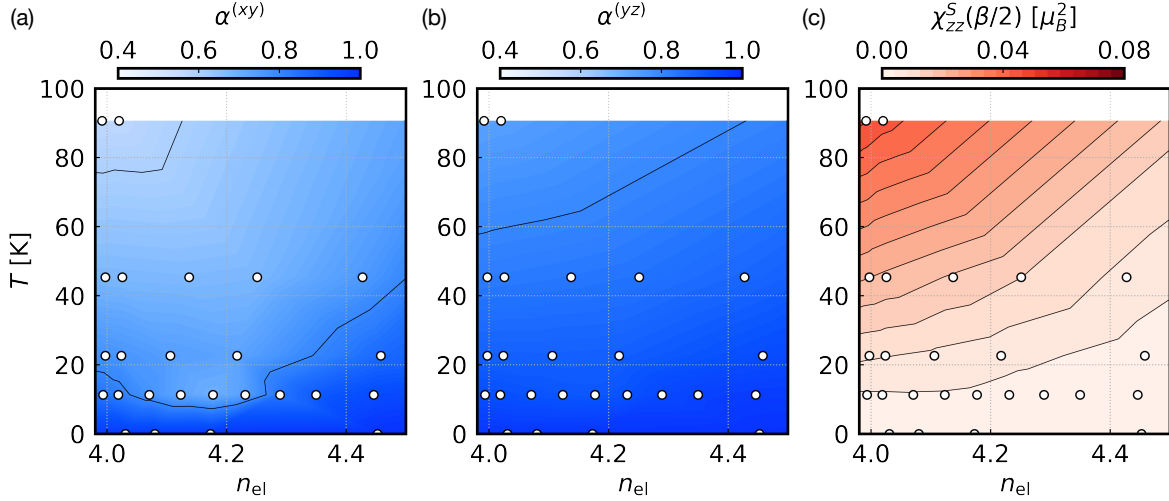


FIG. S4. (a,b) Power exponent α of the imaginary part of the Matsubara self-energy of the d_{xy} component (a) and the d_{yz} component (b). (c) Long-time correlator $\chi_{zz}^S(\tau = \beta/2)$ in the T - n plane.

Fitting bath parameters in the ED solver

One important aspect of the exact diagonalization (ED) solver is how to fit the bath parameters in an impurity model. All the data presented in the main text come from minimizing a non-uniformly weighted cost function, such that

$$\chi^{\text{cost}}(\{\epsilon_l, V_{\mu l}\}) = \sum_n \sum_{\mu\nu} W(i\omega_n) \left| [\mathcal{G}_{0,\text{target}}^{-1}(i\omega_n)]_{\mu\nu} - [\mathcal{G}_0^{-1}(i\omega_n; \{\epsilon_l, V_{\mu l}\})]_{\mu\nu} \right|^2, \quad (\text{S1})$$

where ϵ_l is the l -th bath orbital energy, $V_{\mu l}$ is the hybridization strength between the l -th bath and μ -th correlated orbitals, \mathcal{G}_0^{-1} is a non-interacting Green function, and $W(i\omega_n) = \frac{1}{\mathcal{N}}(\omega_n)^{-\gamma}$ where \mathcal{N} is a normalization constant. We set $\gamma = 1$ to weight low-frequency, which is believed to be more reliable in strongly correlated metals [S5, S8]. We use three (six, considering spin) correlated and nine (eighteen) bath orbitals to satisfy the minimum requirement to describe multi-orbital physics [S8–S12]. Further consideration of the number of bath orbitals, namely, more than three per correlated orbital, is expected not to improve the spectra near the Fermi level but rather the resolution of high-frequency spectra [S11, S12].

* chkim82@snu.ac.kr

† arago@ibs.re.kr

- [S1] J. Mravlje, M. Aichhorn, T. Miyake, K. Haule, G. Kotliar, and A. Georges, Phys. Rev. Lett. **106**, 096401 (2011).
[S2] M. Kim, J. Mravlje, M. Ferrero, O. Parcollet, and A. Georges, Phys. Rev. Lett. **120**, 126401 (2018).
[S3] A. Tamai, M. Zingl, E. Rozbicki, E. Cappelli, S. Riccò, A. de la Torre, S. McKeown Walker, F. Y. Bruno, P. D. C. King, W. Meevasana, M. Shi, M. Radović, N. C. Plumb, A. S. Gibbs, A. P. Mackenzie, C. Berthod, H. U. R. Strand, M. Kim, A. Georges, and F. Baumberger, Phys. Rev. X **9**, 021048 (2019).
[S4] F. B. Kugler, M. Zingl, H. U. R. Strand, S.-S. B. Lee, J. von Delft, and A. Georges, Phys. Rev. Lett. **124**, 16401 (2020).
[S5] N.-O. Linden, M. Zingl, C. Hubig, O. Parcollet, and U. Schollwöck, Phys. Rev. B **101**, 41101 (2020).
[S6] J. Karp, M. Bramberger, M. Grundner, U. Schollwöck, A. J. Millis, and M. Zingl, “Sr₂MoO₄ and Sr₂RuO₄: Disentangling the Roles of Hund’s and van Hove Physics,” (2020), arXiv:2004.12515.
[S7] C. Bergemann, A. P. Mackenzie, S. R. Julian, D. Forsythe, and E. Ohmichi, Adv. Phys. **52**, 639 (2003).
[S8] A. Liebsch and H. Ishida, J. Phys. Condens. Matter **24**, 53201 (2012).
[S9] E. Koch, G. Sangiovanni, and O. Gunnarsson, Phys. Rev. B **78**, 115102 (2008).
[S10] D. Sénéchal, Phys. Rev. B **81**, 235125 (2010).
[S11] A. Go and A. J. Millis, Phys. Rev. Lett. **114**, 016402 (2015).
[S12] E. Fertitta and G. H. Booth, Phys. Rev. B **98**, 235132 (2018).